Glass Performance Days 2025

# Scaling Effects on Post-failure Responses of Laminated Glass Plates under Uniform Pressure

**Sicheng Zhou, Luigi Biolzi, Marco Simonceli, Sara Cattaneo**

Politecnico di Milano, Department of Architecture, Built Environment and Construction Engineering, Milan, Italy. sicheng.zhou@polimi.it

## Abstract

The need for architectural transparency increased the use of glass as structural and non-structural elements (e.g., beams, panels, plates, etc.). Moreover, when canopy and façade panels are employed, the supports are generally realized using small point-fixing steel hinges, which enhance the transparency of the elements bringing non-negligible structural problems. When these elements are employed, different glass plies are coupled together with a polymeric interlayer. The glass plies are subjected to a thermal process to improve their reliability and safety obtaining two different glass typologies: heat-strengthened and thermally toughened laminated glass plates. While in the elastic phase, both glasses perform the same way, the post-breakage response is different due to the very different fragmentations of the ply.

In this study, two full-scale laminated glass (LG) plates, with a global size (L×H) of 4000 mm × 2085 mm, and 2-ply 10 mm thick glass plies coupled with one layer of 1.52 mm thick SentryGlas (SG) interlayer, were investigated under uniform pressure. Different glass plies - heat-strengthened and thermally toughened, damage configurations in glass ply, and size effects were considered. The mechanical response of LG plates was analysed to assess their elastic and post-failure behavior. The findings demonstrate that: (i) the post-failure behavior of LG plates was significantly influenced by the breakage of thermally-toughened glass; (ii) size effects have a great influence on the behavior of LG plates; This effect is particularly pronounced when the fracture occurs in the large-sized LG plate.

## Keywords

Laminated glass plates, Heat-strengthened and thermally toughened glass, Point-fixing; Post-failure behavior; Size effect

## Article Information

- Published by Glass Performance Days, on behalf of the author(s)
- Published as part of the Glass Performance Days Conference Proceedings, June 2025
- Editors: Jan Belis, Christian Louter & Marko Mökkönen

## 1. Introduction

Laminated glass (LG) has become a critical component in architectural and structural applications due to its superior safety performance and residual load-bearing capacity after fracture. Unlike monolithic glass, LG maintains a degree of structural integrity even after cracking, owing to the presence of polymeric interlayers—such as polyvinyl butyral (PVB) or ionoplast—which couple fractured glass fragments and enable continued stress transfer. This post-failure behavior is essential for ensuring occupant safety and system robustness, particularly under accidental or extreme loading conditions.

Recent studies have extensively investigated the mechanical behavior of laminated glass plates, particularly focusing on long term behavior (López-Aenlle et al, 2013; Valarinho et al, 2017), simply-supported (Biolzi et al. 2022a; Biolzi et al. 2022b; Bedon et al, 2025), and post-breakage performance under various boundary conditions (Zemanová et al, 2014; Zemanová et al, 2018; Samieian et al, 2019;) and interlayer types (Serafinavicius et al, 2013; Inca et al, 2022). However, the majority of these investigations have been conducted at laboratory scale, using specimens typically in the range of 0.3–1.2 meters. While such studies provide valuable insights, they do not fully capture the effects of geometrical scaling, which can significantly influence the residual stiffness and post-failure behavior.

Moreover, design models such as the Enhanced Effective Thickness (EET) method (Galuppi & Royer-Carfagni, 2012; López-Aenlle & Pelayo, 2019), while widely adopted, often lack calibration for large-scale fractured configurations. Given that full-scale laminated glass panels in façade and roof systems can exceed several meters in span, understanding scaling effects on post-failure behavior under uniform pressure is vital for the development of reliable, performance-based design methods.

This paper aims to address this gap by investigating the influence of geometric scaling on the post-breakage response of laminated glass plates subjected to uniform pressure. Through a combined experimental and numerical approach, we explore how changes in panel size affect residual load-bearing capacity, deformation profiles, and interlayer engagement. The findings are expected to provide both theoretical and practical contributions to the design and safety assessment of large-scale laminated glass structures.

## 2. Material and Test program

### 2.1. Materials and specimens

The laminated glass plates used in the tests are composed of two 10 mm thick glass plies bonded together with a 1.52 mm thick SentryGlas (SG) interlayer, with a length of 4000 mm and a width of 2085 mm. Two different glass types: thermally-toughened (T) and heat-strengthened glass (I), are employed in this study. And the details are shown in Fig. 1a and Table 1. A systematic designation is adopted to identify each specimen, incorporating the glass type—thermally-toughened (T) or heat-strengthened (I), a consistent glass thickness of 10 mm, the interlayer type—SentryGlas (S), and the plate size—large (L).

*Table 1: Details of the specimen.*

| Specimen Tag | Size of the laminated glass plates | | | |
|---|---|---|---|---|
| | $s_W$ | $s_L$ | $W$ | $L$ |
| [-] | [mm] | [mm] | [mm] | [mm] |
| T10S-L | 1800 | 1800 | 2085 | 4000 |
| I10S-L | 1800 | 1800 | 2085 | 4000 |

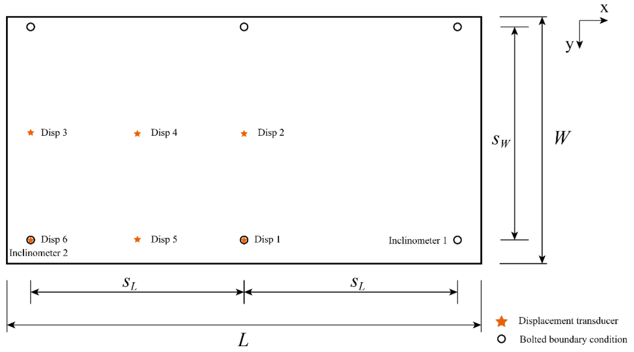


*(a) Details of specimens*

*(b) Photo of the test setup*

*Fig. 1: Details of the tested specimens and setup.*

## 2.2. Test program

**Experimental program**

The static test setup is shown in Fig. 1b. The front edge of the laminated glass panels was connected to steel ropes, which were tensioned and anchored to a rigid counter frame. The rear edge was supported by cylindrical steel pins, allowing rotation about the x-axis, and fixed to a rigid concrete block to ensure stable boundary conditions. Front hinges were located 200 mm from the plate edges, with a longitudinal distance $s_W$ to the rear hinges. Four-point fixing boundary condition was considered in this study. This configuration replicates point-fixed laminated glass panels typically used in parapets and canopies.

Experimental tests were performed on point-fixed laminated glass (LG) plates under a uniformly distributed load of $1\mathrm{KN/m^2}$, applied using sandbags and counterweights with a total equivalent load of $8340\ \mathrm{N}$ (as shown in Fig. 1b). Deformation was measured using three draw-wire sensors and three LVDTs, recorded via a data acquisition system. The locations of sensors used in this study are shown in Fig. 1a.

This study investigates the post-failure behavior of point-fixed laminated glass plates under out-of-plane uniform pressure. Three configurations were tested: undamaged plates (Configuration 0), plates with the bottom ply intentionally fractured prior to loading (Configuration I), and the same specimens flipped upside down before loading (Configuration II). It should be noted that no uniform load was applied in Configuration I due to its large initial deformation induced by the breakage of bottom glass ply and self-weight. The configurations are illustrated in Fig. 2.

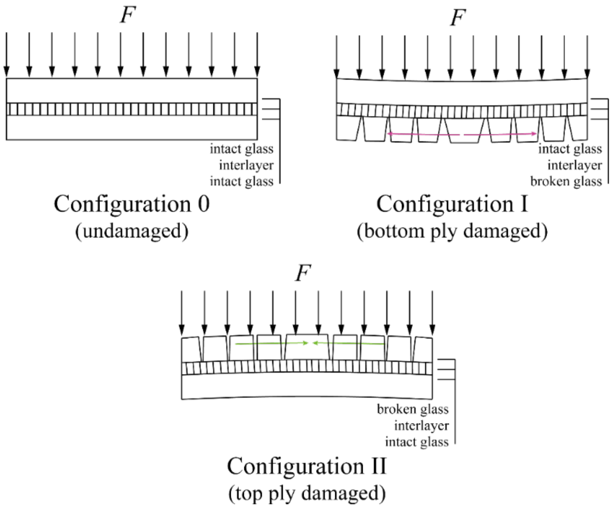


*Fig. 2: Different damage configurations of laminated glass plates (Biolzi et al, 2025).*

**Numerical program**

To study the global response of point-fixed laminated glass plates, full-scale numerical models were developed in ABAQUS, as shown in Fig. 3. Considering the high length-to-thickness ratio (>100), specimens were modelled as 3D shell composites for efficiency and accuracy. The model included two glass plies and one SG interlayer, with nine integration points through the interlayer thickness. All materials were assumed linear elastic, defined by their elastic modulus and Poisson's ratio following (Biolzi et al, 2010).

Numerical simulations employed a four-point fixing configuration replicating experimental boundary conditions via control nodes and connector elements. One long edge was fully constrained at drilled holes (UX, UY, UZ, UR3), while the opposite edge was connected to a hinge-simulating AISI rod, allowing rotation about the x-axis (UR1) only.

Laminated glass (LG) plates were modeled using S4R shell elements; supporting rods were modeled as B31 beam elements. A structured mesh was applied, with element size equal to the glass ply thickness in the through-thickness direction and twice the thickness in-plane. Local refinement was implemented around fixing holes to capture stress concentrations. Glass and interlayer were rigidly bonded, assuming no delamination, consistent with experimental observations. To simulate post-breakage behavior, an equivalent elastic modulus was assigned to the fractured glass ply (Bedon et al, 2025), preserving its residual stiffness contribution.

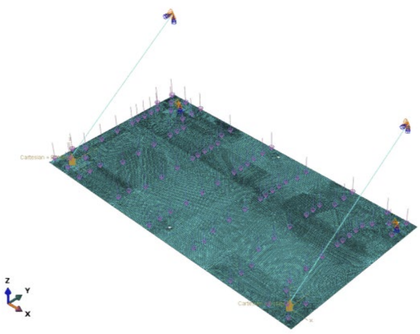

*Fig. 3: 3D view of the finite element model of the considered LG plates.*

# 3. Results

The static response of the laminated glass plates with different damage configurations under uniform pressure was studied in this section. The load was applied by sequentially adding sandbags and iron counterweights, and this could make the raw load–displacement curve exhibit a sawtooth pattern. Therefore, a quadratic curve fitting method was applied to smooth the data for clearer representation. Deformation data were time-synchronized with the applied load to ensure accuracy. The displacement at 'Disp1' (as shown in Fig. 1) —consistently the maximum among all measured points—was selected as the representative deformation.

## 3.1. Experimental results

The mechanical response of undamaged large-sized LG plates with four-point fixing boundary conditions is illustrated in Fig. 4. The two specimens exhibit similar overall load–displacement responses, with maximum displacements of 39.98 mm (T10S-L) and 38.62 mm (I10S-L), respectively. Both curves show a near-linear trend. However, notable differences are observed in the residual deformation after unloading, with residual displacements of 0.40 mm (T10S-L) and 8.99 mm (I10S-L). This could be explained by the rotation of the articulated fixing point, as discussed previously in Biolzi et al (2024).

Photo of the test

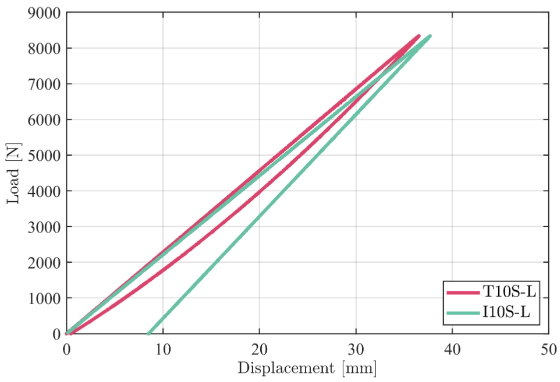


Load vs. Displacement

*Fig. 4: Results of Configuration 0*

In Configuration I, the bottom ply of the laminated glass plates was broken by a glass breaker. Fracture was induced under six-point fixing to prevent uncontrolled failure and material loss, particularly in thermally-toughened glass, due to strain energy release and self-weight effects. After the hitting, a transient displacement was observed due to the release of the stored mechanical energy in the glass. Experimental results indicate that LG plates composed of thermally-toughened glass exhibited greater displacement upon bottom ply fracture compared to those made of heat-strengthened glass, as shown in Fig. 5. Upon the fracture occurring, thermally-toughened glass exhibited uniformly distributed fine fragments, while heat-strengthened glass displayed fewer, larger crack paths, resulting in coarser fragmentation.

For large specimens under four-point fixing, the fracture of the bottom glass ply combined with self-weight induced significant displacement exceeding 140 mm. To avoid catastrophic failure, no additional uniform load was applied in Configuration I for these specimens.

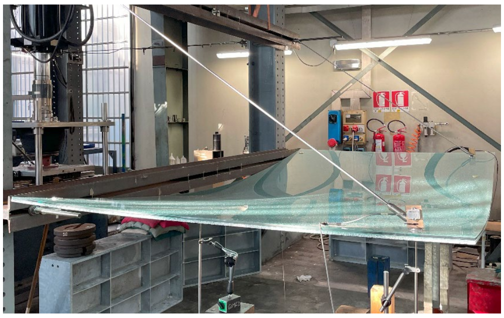

T10S-L

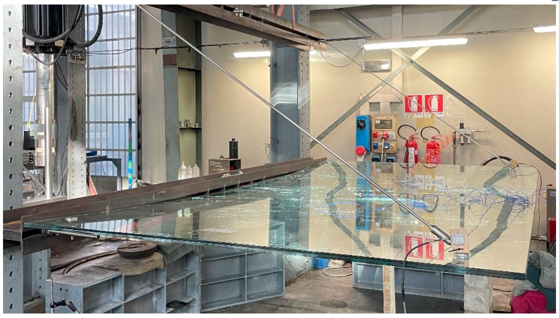

I10S-L

*Fig. 5: Deformed shape of LG specimens at the onset of bottom ply fracture.*

Configuration II was established by flipping the deformed LG plates tested in Configuration I (as shown in Fig. 6a), resulting in an initial curvature opposite to the loading direction. This pre-deformation was notably pronounced in thermally toughened glass, while being negligible in heat-strengthened glass. LG plates in Configuration II exhibited slight nonlinearity in the load–displacement response, with maximum displacements of 40.65 mm and 44.26 mm recorded at the 'Disp 1' location.

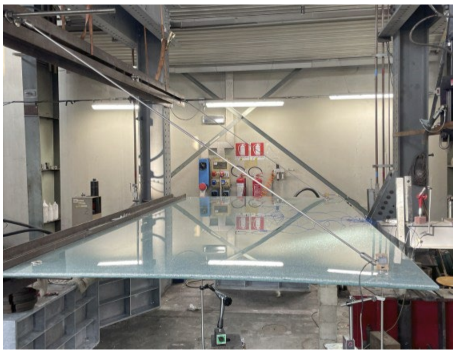

Photo of the initial deformation of T10S-L

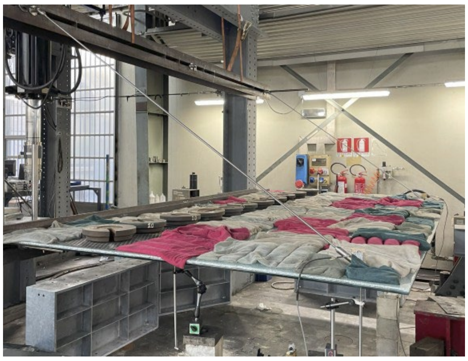

Photo of the test on T10S-L

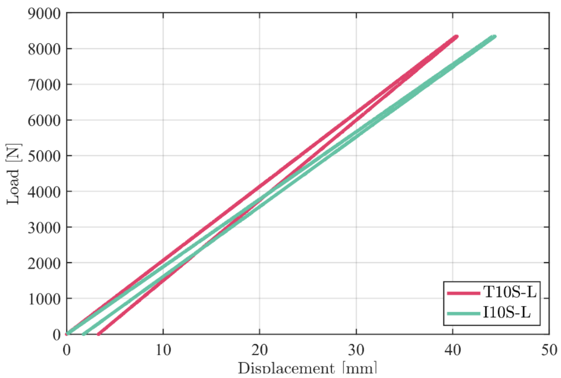


Load Vs. displacement

*Fig. 6: Results of Configuration II*

*Table 2: Summary of experimental results*

| | Disp 1 | | Disp 2 | | Disp 4 | | Disp 5 | |
|---|---|---|---|---|---|---|---|---|
| | $d_{max}$ | $d_{rel}$ | $d_{max}$ | $d_{rel}$ | $d_{max}$ | $d_{rel}$ | $d_{max}$ | $d_{rel}$ |
| Units: | [mm] | [mm] | [mm] | [mm] | [mm] | [mm] | [mm] | [mm] |
| Configuration 0 | | | | | | | | |
| T10S-L | 39.98 | 0.40 | 36.63 | 0.44 | 28.63 | 2.37 | 29.20 | 0.38 |
| I10S-L | 38.62 | 8.99 | 37.91 | 8.50 | 29.87 | 6.18 | 28.36 | 4.78 |
| Configuration II | | | | | | | | |
| T10S-L | 40.65 | 1.80 | 36.97 | 3.50 | 32.73 | 4.85 | 28.34 | 1.63 |
| I10S-L | 44.26 | 0.60 | 41.71 | 1.70 | 33.24 | 2.69 | 32.95 | 1.53 |

## 3.2. Numerical results

For both thermally toughened and heat-strengthened glass, a single numerical model was developed for each glass type in Configurations 0 and II. The elastic modulus of glass was adopted as 70 GPa in Configuration 0. On the other hand, the fractured glass ply was represented in this study using an equivalent elastic modulus of 45 GPa in Configuration II. The results, summarized in Fig. 7 and Table 3, were evaluated using the absolute relative difference (ARD) to quantify the deviation between simulations and experiments, which was defined as follows:

$$ARD = \left|\frac{d_{ex}-d_{nu}}{d_{nu}}\right| \tag{1}$$

In high-displacement regions, the ARD remained within 5%, indicating strong agreement between numerical and experimental data. In low-displacement zones near the supports, differences of approximately 10% were observed, which are considered acceptable. The predicted deformed shapes closely matched experimental observations, particularly the slightly higher displacement at the front-central region (‘Disp 1’) under four-point fixing.

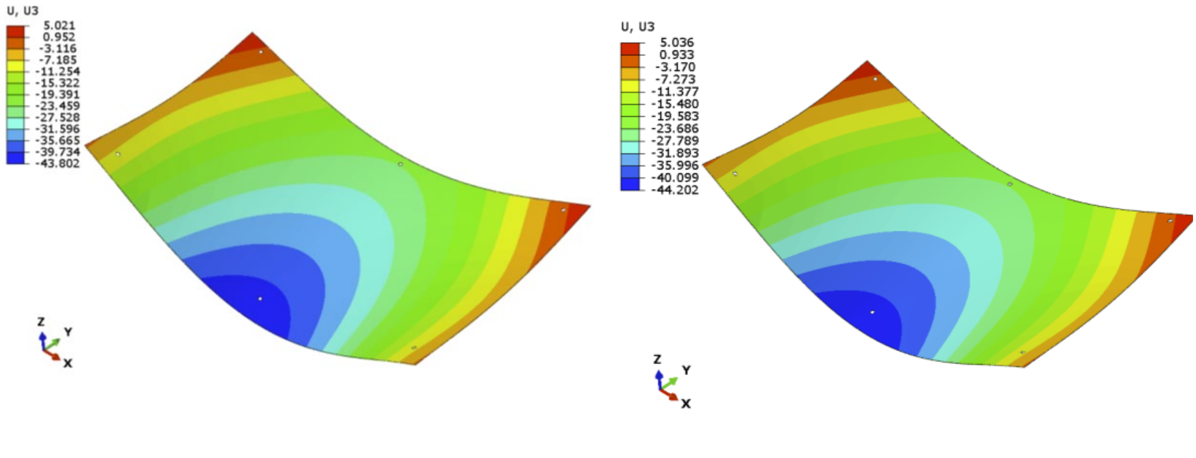


Configuration 0 Configuration II

*Fig. 7: Deformed shape of numerical model.*

Table 3: Comparison of Numerical and Experimental Displacement Results.

| | Disp 1 | | | Disp 2 | | | Disp 5 | | |
|---|---|---|---|---|---|---|---|---|---|
| | $d_{ex}$ [mm] | $d_{nu}$ [mm] | ARD [%] | $d_{ex}$ [mm] | $d_{nu}$ [mm] | ARD [%] | $d_{ex}$ [mm] | $d_{nu}$ [mm] | ARD [%] |
| Configuration 0 | | | | | | | | | |
| T10S-L | 39.98 | 40.84 | 2.2 | 36.63 | 35.56 | 2.9 | 29.20 | 31.50 | 7.9 |
| I10S-L | 38.62 | 40.84 | 5.7 | 37.91 | 35.56 | 6.2 | 28.36 | 31.50 | 11.0 |
| Configuration II | | | | | | | | | |
| T10S-L | 40.65 | 40.11 | 1.3 | 36.97 | 36.00 | 2.6 | 28.34 | 29.71 | 4.8 |
| I10S-L | 44.26 | 40.11 | 9.4 | 41.71 | 36.00 | 13.7 | 32.95 | 29.71 | 9.8 |

## 4. Discussion

A comprehensive summary of the stiffness values for all tested specimens is presented in Table 4. It should be noted the results of current study are also compared with the results in previous study (Biolzi et al, 2025), with the size of plates of 2200 mm × 2085 mm (with the caption of ‘M’: medium-sized). Regardless of specimen size or damage location, the use of thermally toughened glass consistently resulted in a marked reduction in stiffness following damage. In contrast, heat-strengthened glass exhibited greater stability: the stiffness of medium-sized specimens remained virtually unaffected, whereas a notable reduction was observed in large-sized specimens. The results highlight the influence of specimen size on the distinct post-damage mechanical response of laminated glass (LG) plates under four-point fixing. Medium-sized specimens (M) consistently demonstrated higher normalized stiffness (load / displacement, N/mm) compared to large-sized specimens across all configurations.

In Configuration 0 (undamaged state), the T10S-M and I10S-M specimens exhibited stiffness values of 479.26 N/mm and 457.80 N/mm, respectively, while their large-sized counterparts, T10S-L and I10S-L, showed significantly reduced values of 290.40 N/mm and 287.70 N/mm. This reduction—approximately 39% for T10S and 37% for I10S—highlights the size-dependent flexibility of the LG plates, where increased span length amplifies deflection under equivalent loading conditions.

In Configuration II, following bottom ply fracture and plate flipping, the size effect remains evident. T10S-L and I10S-L exhibited stiffness reductions of 34.51% and 28.16%, respectively, compared to their Configuration 0 counterparts. Notably, the stiffness reduction from M to L specimens is more pronounced for thermally toughened glass, suggesting greater sensitivity to geometrical nonlinearity and post-breakage deformation in larger spans.

These findings underscore the importance of considering plate size in the design and performance assessment of point-fixed laminated glass structures. Larger panels, while offering greater coverage, exhibit reduced stiffness and higher post-fracture displacements, which may impact serviceability and residual load-bearing capacity.

*Table 4: Summary of stiffness of experimental results.*

| Specimen | Configuration 0 | Configuration I | Configuration II |
|---|---|---|---|
| Units | [N / mm] | [N / mm] | [N / mm] |
| T10S-M * | 479.26 | 373.60 (-22.05%) | 384.00 (-19.88%) |
| I10S-M * | 457.80 | 441.23 (-3.62%) | 439.23 (-4.06%) |
| T10S-L | 290.40 | - | 190.18 (-34.51%) |
| I10S-L | 287.70 | - | 206.67 (-28.16%) |

Note: Specimens marked with * are sourced from a previous study. Specifically, T10S-M and I10S-M in this study correspond to 10T-SG and 10I-SG, respectively, in the previous work.

## 5. Conclusions

This study investigated the mechanical response of point-fixing laminated glass (LG) plates under out-of-plane uniform pressure, considering different damage configurations, glass types, and specimen sizes. Experimental and numerical results consistently demonstrated that thermally toughened glass exhibits a pronounced reduction in stiffness after damage, regardless of plate size. In contrast, heat-strengthened glass showed greater post-damage stiffness retention, particularly in medium-sized specimens.

A significant size effect was observed: large specimens displayed notably lower stiffness compared to medium-sized ones, emphasizing the importance of geometric scale in design considerations. Numerical simulations aligned closely with experimental findings, validating the modeling approach and providing insight into the post-fracture mechanical behavior of LG plates. These outcomes contribute to the optimization of laminated glass design in architectural applications, particularly in safety-critical elements such as parapets and canopies.

## Acknowledgements

The research is sponsored by China Scholarship Council, with CSC NO. 202108330086.

## References

Bedon, C., Kozłowski, M., & Cella, N. (2025). Gaps in the post-breakage out-of-plane bending stiffness assessment of 2-ply partially damaged laminated glass elements under short-term quasi-static loads. Engineering Structures, 327, 119617. Retrieved from: https://doi.org/10.1016/j.engstruct.2025.119617

Biolzi, L., Cattaneo, S., & Rosati, G. (2010). Progressive damage and fracture of laminated glass beams. Construction and Building Materials, 24(4), 577-584. Retrieved from: https://doi.org/10.1016/j.conbuildmat.2009.09.007

Biolzi, L., & Simoncelli, M. (2022a). Overall response of 2-ply laminated glass plates under out-of-plane loading. Engineering Structures, 256, 113967. Retrieved from: https://doi.org/10.1016/j.engstruct.2022.113967

Biolzi, L., Cattaneo, S., & Simoncelli, M. (2022b). Post-failure behavior of 2-ply laminated glass plates with different interlayers. Engineering Fracture Mechanics, 268, 108496. https://doi.org/10.1016/j.engfracmech.2022.108496

Biolzi, L., Simoncelli, M., & Zhou, S. (2025). Static and dynamic responses of point-fixing laminated glass plates under out-of-plane loading. Engineering Structures, 325, 119409. https://doi.org/10.1016/j.engstruct.2024.119409

Galuppi, L., & Royer-Carfagni, G. (2012). The effective thickness of laminated glass plates. Journal of Mechanics of Materials and Structures, 7(4), 375-400. Retrieved from: https://doi.org/10.2140/jomms.2012.7.375

Inca , E., Jordão , S., Bedon , C., Mesquita , A., & Rebelo , C. (2022). Numerical Analysis of Laminated Glass Panels with Articulared Bolted Point Fixings. ce/papers, 5(2), 140-149. https://doi.org/10.1002/cepa.1709

López-Aenlle, M., Pelayo, F., Fernández-Canteli, A., & Prieto, M. G. (2013). The effective-thickness concept in laminated-glass elements under static loading. Engineering structures, 56, 1092-1102. Retrieved from: https://doi.org/10.1016/j.engstruct.2013.06.018

López-Aenlle, M., & Pelayo, F. (2019). Static and dynamic effective thickness in five-layered glass plates. Composite Structures, 212, 259-270. Retrieved from: https://doi.org/10.1016/j.compstruct.2019.01.037

Samieian, M. A., Cormie, D., Smith, D., Wholey, W., Blackman, B. R., Dear, J. P., & Hooper, P. A. (2019). On the bonding between glass and PVB in laminated glass. Engineering Fracture Mechanics, 214, 504-519. Retrieved from: https://doi.org/10.1016/j.engfracmech.2019.04.006

Serafinavicius, T., Kvedaras, A. K., & Sauciuvenas, G. (2013). Bending behavior of structural glass laminated with different interlayers. Mechanics of composite materials, 49, 437-446. https://doi.org/10.1007/s11029-013-9360-4

Valarinho, L., Correia, J. R., Garrido, M., Sá, M., & Branco, F. (2017). A. Flexural creep behavior of full-scale laminated glass panels. Journal of Structural Engineering, 143(10), 04017139. https://doi.org/10.1061/(ASCE)ST.1943-541X.0001841

Zemanová, A., Zeman, J., & Šejnoha, M. (,2014). Numerical model of elastic laminated glass beams under finite strain. Archives of Civil and Mechanical Engineering, 14, 734-744. https://doi.org/10.1016/j.acme.2014.03.005

Zemanová, A., Zeman, J., Janda, T., Schmidt, J., & Šejnoha, M. (2018). On modal analysis of laminated glass: Usability of simplified methods and Enhanced Effective Thickness. Composites Part B: Engineering, 151, 92-105. Retrieved from: https://doi.org/10.1016/j.compositesb.2018.05.032